NANO LETTERS
Cite This: Nano Lett. XXXX, XXX, XXX−XXX
Letter
pubs.acs.org/NanoLett

Nano-electromechanical Drumhead Resonators from Two-Dimensional Material Bimorphs

SunPhil Kim,* Jaehyung Yu, and Arend M. van der Zande*

Department of Mechanical Science and Engineering, University of Illinois at Urbana−Champaign, Urbana, Illinois 61801, United States

Supporting Information

ABSTRACT: Atomic membranes of monolayer 2D materials represent the ultimate limit in the size of nano-electromechanical systems. However, new properties and new functionalities emerge by looking at the interface between layers in heterostructures of 2D materials. Here, we demonstrate the integration of 2D heterostructures as tunable nano-electromechanical systems, exploring the competition between the mechanics of the ultrathin membrane and the incommensurate van der Waals interface. We fabricate electrically contacted 5 or 6 μm circular drumheads of suspended heterostructure membranes of monolayer graphene on monolayer molybdenum disulfide (MoS_2), which we call a 2D bimorph. We characterize the mechanical resonance through electrostatic actuation and laser interferometry detection. The 2D bimorphs have resonance frequencies of 5−20 MHz and quality factors of 50−700, comparable to resonators from monolayer or few-layer 2D materials. The frequencies and eigenmode shapes of the higher harmonics display split degenerate modes, showing that the 2D bimorphs behave as membranes with asymmetric tension. The devices display dynamic ranges of 44 dB, with an additional nonlinearity in the dissipation at small drive. Under electrostatic frequency tuning, devices display a small tuning of ~20% compared with graphene resonators, which have >100%. In addition, the tuning shows a kink that deviates from the tensioned membrane model for atomic membranes and corresponds with a changing in stress of 14 mN/m. A model that accounts for this tuning behavior is the onset of interlayer slip in the heterostructure, allowing the tension in the membrane to relax. Using density functional theory simulations, we find that the change in stress at the kink is much larger than the predicted energy barrier for interlayer slip of 0.102 mN/m in an incommensurate 2D heterostructure but smaller than the energy barrier for an aligned graphene bilayer of 35 mN/m, suggesting a local pinning effect at ripples or folds in the heterostructure. Finally, we observe an asymmetry in tuning of the full width at half-maximum that does not exist in monolayer resonators. These findings demonstrate a new class of nano-electromechanical systems from 2D heterostructures and unravel the complex interaction of membrane morphology versus interlayer adhesion and slip on the mechanics of incommensurate van der Waals interfaces.

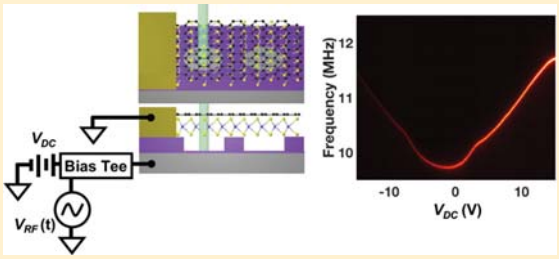

KEYWORDS: *2D materials, mechanical resonator, bimorph, NEMS, 2D heterostructure, nonlinear dynamics*

Due to their unparalleled mechanical strength[1,2] and stability down to a monolayer, atomically thin membranes made from two-dimensional (2D) materials such as graphene and MoS_2 represent the ultimate limit in size of nano-electromechanical systems (NEMS).[3−7] However, many of the most interesting properties of 2D materials and new functionality arise from the interfaces between layers and in engineering multilayer heterostructures. The past few years have led to a revolution in nano-electronics from 2D heterostructures, in which layer-by-layer stacking of monolayer 2D materials with disparate electronic properties leads to functional nanometer scale electronic devices.[8−10] An open question is how to integrate the outstanding mechanical properties of 2D materials with the enhanced functionality of heterostructures to enable new technologies such as 3D foldable circuitry, nanoscale origami, or resonant NEMS utilizing 2D heterostructures as active electronic and mechanical components.

As mechanically robust and electrically active monolayers, suspended membranes from 2D materials are highly responsive and tunable resonators, making them excellent candidates for next generation NEMS, such as tunable filters,[4,7] oscillators,[11] switches,[12] piezotronics,[13] and mass and force sensors.[7,14] In addition, the atomic thickness in NEMS made from 2D materials leads to emergent mechanics such as high-size-dependent dissipation,[6] strong nonlinearity,[15] stochastic frequency broadening,[16] ultrahigh Q at low temperatures,[4,7,17] and optomechanical heating and cooling.[18] However, many technologies in nano- and micro-electromechanical systems need more than one layer to enable operation. For example, a bimorph is a ubiquitous element in MEMS sensors and actuators that relies on the differential stress between two layers with

Received: May 11, 2018
Revised: October 10, 2018
Published: October 19, 2018

DOI: 10.1021/acs.nanolett.8b01926
Nano Lett. XXXX, XXX, XXX−XXX

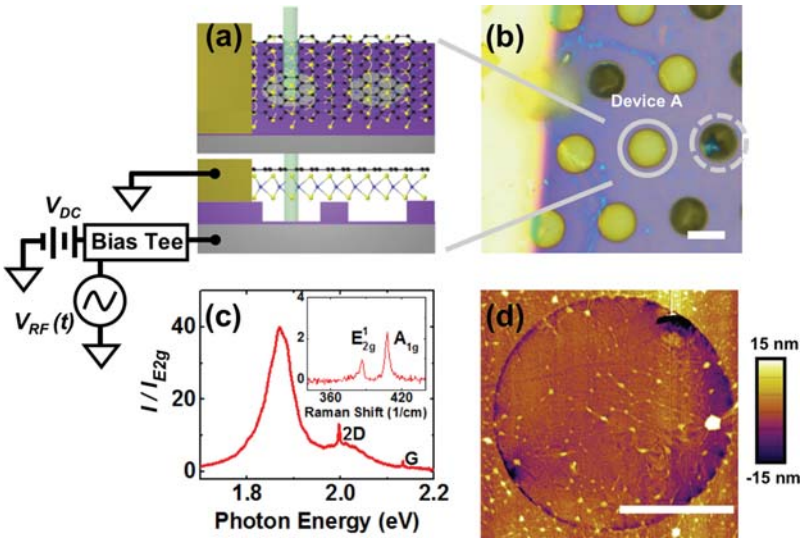

Figure 1. (a) Schematic drawing of a 2D bimorph device and measurement setup. Electrically contacted graphene−MoS_2 heterostructures are suspended as a circular drumhead resonator, actuated electrostatically and measured optically. (b) Optical image of a 2D bimorph membranes suspended over 6 μm pits in a silicon oxide surface. The dotted circle highlights a collapsed membrane, while the solid circle highlights a suspended membrane. Scale bar: 6 μm. (c) Photoluminescence and Raman spectrum of the circled bimorph membrane, showing the characteristic spectrum for both graphene and MoS_2. The inset is the measured MoS_2 Raman spectrum. (d) Atomic-force micrograph showing the topography of the circled membrane. The suspended membrane has small ripples and there are bubbles at the interface between the graphene and MoS_2 layers with heights ranging from 1 to 15 nm. The AFM was captured after all resonance measurements were completed. Scale bar: 3 μm.

different properties. As a recent demonstration, origami bimorphs from nanometer-thick graphene and ALD silicon dioxide were made to actuate and fold due to electrochemical signals.[19] In addition, heterostructures enable new methods of transduction and new physics. For example, there was a recent demonstration of a resonator composed of a 2D heterostructure of $NbSe_2$ encapsulated by graphene layers, which showed high quality factors of 245 000 and enhanced transduction from reduced resistivity at low temperatures.[20] Critical questions for the realization of many of the potential applications are what the impact of the van der Waals interface will be on the mechanics of heterostructures and how those mechanics will affect the functionality of NEMS based entirely on 2D heterostructures.

While engineering NEMS from 2D heterostructures is a recent area of study, in the field of nanotribology, the mechanics of van der Waals interfaces has been studied for decades. When 2D layers are incommensurate through twist, strain, or different lattice constant, friction from van der Waals interactions become negligible, leading to interlayer superlubricity and slip.[21−24] There have been direct observations of slip at van der Waals interfaces misaligned graphene nanoflakes as well as other 2D materials or mesas over a graphite substrate.[25−28] These studies predict that 2D heterostructures will also exhibit interlayer slip,[29,30] but the impact of this slip on the mechanics of a heterostructure membrane is not well-understood, which should lead to a dramatic impact on the mechanics of a heterostructure membrane. Slip events have been observed through nanoindentation on membranes of an aligned, commensurate bilayer or few-layer graphene.[31,32] Similar nanoindentation of 2D heterostructures reveal that the elastic moduli of the heterostructures are less than the sum of their components,[33] while mechanical resonance of few layer 2D heterostructures show that resonance frequencies lie between the values of pure graphene or pure MoS_2 resonators.[34] However, these studies do not reveal the origin of this softening, nor do they observe any indication of interface interaction such as interlayer slip. The goal of this study is to determine when conventional membrane mechanics or interlayer interactions at the incommensurate van der Waals interface will dominate the resonance properties of atomic membranes made from 2D heterostructures.

In this study, we demonstrate electrically integrated nanoelectromechanical resonators from heterostructures of 2D materials by fabricating a suspended drumhead membrane from a heterostructure of monolayer graphene on monolayer molybdenum disulfide (MoS_2). This structure is the simplest electromechanical device from a 2D heterostructure: a two-molecule-thick bimorph that will hereafter be referred to as a 2D bimorph. Unlike conventional bimorphs, the 2D materials are only held together through weak van der Waals interactions, enabling us to probe the mechanics of this interface. We use mechanical resonance to compare the behavior of the 2D bimorphs to resonators from monolayer 2D materials. We measure the resonance frequencies, eigenmodes, and tuning behavior of the resonators. From the resonance frequencies and eigenmodes measurements, we find that the 2D bimorphs show similar properties to monolayer or few-layer materials, behaving as membranes with asymmetric in-plane tension. This asymmetric tension could easily come from strain induced in the transfer process. However, when measuring the electrostatic tuning of the resonators, we observe distinct kinks in the tuning curve that lead to a strong softening of the frequency as well as an asymmetric tuning of the quality factor, characteristics that are not observed in monolayer or few-layer materials.

The structure of the 2D bimorph is shown in Figure 1. Figure 1a shows a schematic of the device geometry as well as the electrical circuit used for actuation and tuning, while Figure 1b shows an optical image of an array of fabricated bimorph devices. The 2D bimorphs are suspended as circular drumhead membranes over prefabricated 5 or 6 μm diameter holes etched to 230 nm deep in a 285 nm thick silicon oxide epilayer on a degenerately doped silicon substrate. In all membranes, the graphene is on top, while the MoS_2 is on the bottom. The

DOI: 10.1021/acs.nanolett.8b01926
Nano Lett. XXXX, XXX, XXX−XXX

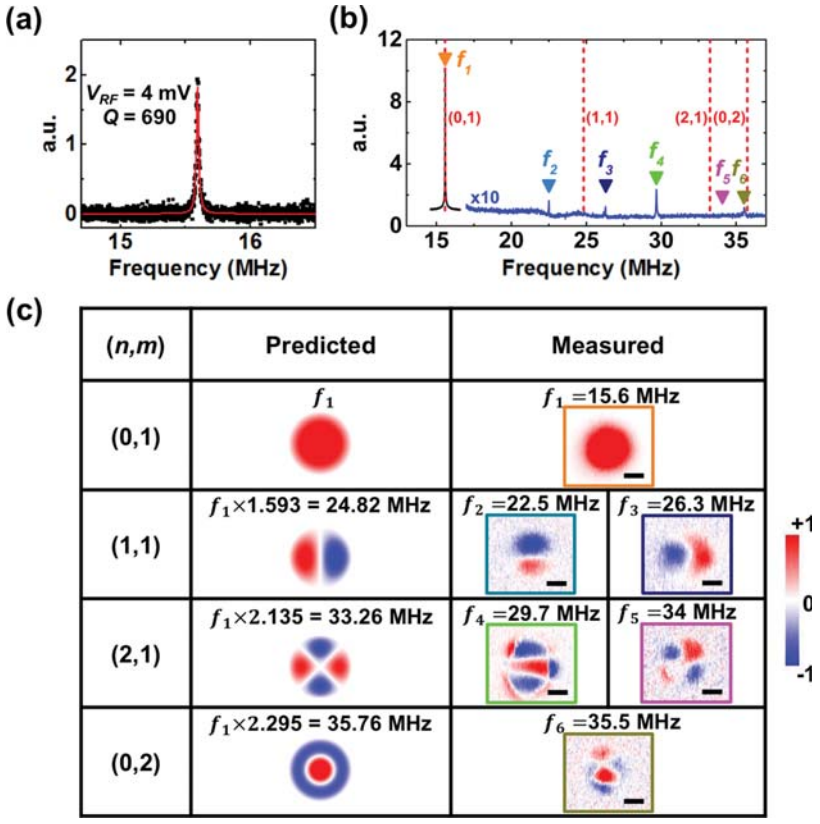

Figure 2. (a) Fundamental resonance of a 5 μm diameter 2D bimorph measured at V_{DC} = 15 V, V_{RF} = 4 mV, and a laser power of 50 μW. The red line is the Lorentzian fit to the data, giving a resonance frequency of 15.6 MHz and a quality factor of 690. (b) Measured fundamental and higher harmonics of the same 2D bimorph measured at V_{DC} = 15 V and V_{RF} = 0.1 V (black) and 0.3 V (blue). The arrows indicate the individual resonances, while the red dotted lines represent the theoretical predictions for higher harmonics based on the first resonance. (c) The predicted and measured eigenmodes for the (0,1), (1,1), (2,1), and (0,2) mechanical resonances. Scale bars: 2 μm.

bimorphs were fabricated by first growing large-area monolayer graphene on copper foil and MoS_2 on silicon oxide using established chemical vapor deposition recipes.[35−37] The graphene was then transferred off the growth substrate and onto the MoS_2 using a sacrificial poly(methyl methacrylate) (PMMA) film with polydimethylsiloxane backing. Note that PMMA is only applied to the top side of graphene, leaving graphene-MoS_2 interface free of any polymer. The entire heterostructure was delaminated from the MoS_2 growth substrate using KOH, rinsed in DI water and then dry-transferred in the air onto the prefabricated holes. The sacrificial polymers were then annealed away in a forming gas at 350 °C for 4 h to leave suspended membranes in a solvent-free process. Finally, electrodes were patterned by metal deposition (2 nm Cr/80 nm Au) through a shadow mask to locally contact the membrane. Additional material growth, transfer, and device-fabrication details are in section 1 of the Supporting Information. As seen in Figure 1b, changes in color due to changes in thin-film optical interference make the suspended membranes (yellow) easily visible compared with empty holes (dark). The gold color on the left is the local metal electrode. As a result, it is easy to identify potential devices for study. There are isolated contaminants on the surface (blue lines in Figure 1b), which are residues that does not get annealed away during the transfer. We only choose devices to study that are visibly free of contaminants.

We used optical spectroscopy (Figure 1c) and atomic force microscopy (AFM) (Figure 1d) to confirm the bimorph structure and to establish the topography and interface quality of the suspended membrane. Figure 1c shows the Raman and photoluminescence (PL) spectrum acquired from the device circled in Figure 1b using a 2.33 eV (532 nm) laser excitation. The two signals are superimposed, so both are plotted together versus energy. The Raman G peak from the graphene is visible at 2.13 eV, while the 2D peak is visible at 2.0 eV. There is no visible D peak, indicating that the graphene membrane has a low defect density. The optical band transition of semiconducting MoS_2 is visible as a photoluminescence peak at 1.86 eV. Figure 1c inset shows the MoS_2 Raman peaks of the E^1_{2g} and A_{1g}. All of the peak intensities are normalized to the E^1_{2g} peak. The intensity of the photoluminescence peak is weak, <20% of the as-grown MoS_2, which is likely a result of the established quenching effect due to energy transfer from the MoS_2 into the graphene that indicates a clean interface between the two materials.[38,39]

Figure 1d shows an AFM topography image of the same membrane. The membrane is suspended and clamped over the entire etched hole. There are bubbles with 1 to 15 nm heights formed at the junction of the graphene−MoS_2 membranes. These bubbles are common in 2D heterostructure devices[40−43] and are likely due to small amounts of residue trapped within the van der Waals interface during transfer. These bubbles emerge when there are either differences in the initial stress of each layer or when small amounts of gas or residue are trapped at the interface and are squeezed out by the van der Waals force into isolated regions.[44−46] The presence of the bubbles is evidence of good adhesion and a clean interface in the regions between the

DOI: 10.1021/acs.nanolett.8b01926
Nano Lett. XXXX, XXX, XXX−XXX

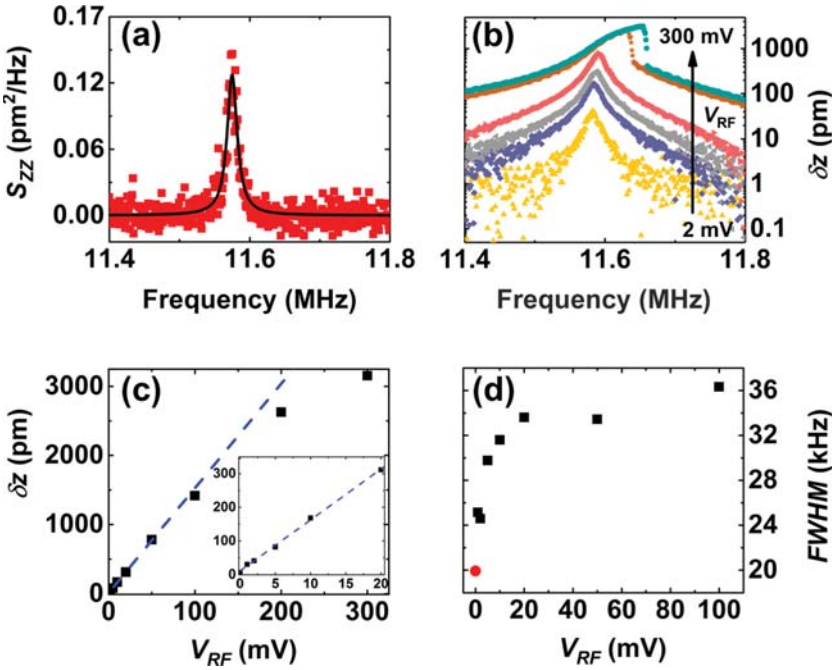

Figure 3. (a) Thermal amplitude noise power density vs frequency obtained with BW = 1 kHz. Black curve is the fit to $S_{ZZ}(f)$. (b) Calibrated amplitude response of the mechanical resonance of a 2D bimorph with respect to increased drive (laser power: 50 μW; V_{DC} = 15 V). (c) Extracted resonance amplitude vs drive. Inset shows the amplitude at low drive. The blue dashed line is the linear fit. (d) Full width at half-maximum (fwhm) from the Lorentzian fit vs drive signal. The red circle represents fwhm from the Brownian motion.

bubbles.[44,45] Additionally, Figure S1 shows images of the materials through the fabrication steps and an AFM at the edge of the heterostructure showing a step height of 0.77 nm between the graphene and graphene−MoS_2, indicating that the interface is clean between bubbles. There are long-range ripples emanating from the bubbles and anisotropies in the clamping, which will affect the uniformity of tension within the membrane. As shown in Figure S2, other membranes measured show the same bubbles, although the size and density vary between membranes.

Figure 1a also outlines the setup used for electromechanical measurements. Applying a static voltage to the silicon back gate leads to electrostatic attraction, tensioning the membrane, while applying a MHz frequency oscillating voltage with a spectrum analyzer will actuate the membrane to resonate. The mechanical motion is then detected by measuring the dynamic optical reflectance of a 520 nm diode laser focused on the membrane (full measurement setup shown in Figure S3). Due to Fabry−Pérot interferometry, the reflected light is modulated by the change in position of the membrane with respect to the reflecting silicon back gate. The laser is controlled with a confocal scan-mirror system, which allows the laser spot to either be fixed at the center of the membrane while the drive frequency is swept with a spectrum analyzer to measure the resonance mode or the laser spot is rastered over the membrane at a fixed modulation frequency to measure the position-dependent eigenmodes. All measurements were performed in an optical cryostat at room temperature in a vacuum with a pressure of $<5 \times 10^{-6}$ Torr.

Figure 2 shows the mechanical resonance and eigenmodes of a suspended 2D bimorph. Figure 2a shows the measured dynamic optical reflection, proportional to the amplitude of motion, versus frequency for the fundamental mode of a resonator at a fixed gate voltage of 15 V and a drive voltage of 4 mV. The resonance frequency and the quality factor of the fundamental mode are 15.58 MHz and 690, respectively. Other devices with the same diameter display variations in frequency and quality factor that range from 5 to 20 MHz and from 50 to ∼700, respectively. These variations in frequency and quality factor are similar to those reported in the literature for monolayer materials[3,4] and can be attributed to variations in the built-in tension and density due to variations in membrane mass resulting from fabrication.

Figure 2b shows the higher harmonics of the same device. The device displays six resonances from 15 to 36 MHz. Assuming that the bimorph behaves as a tensioned drumhead membrane, these higher-order modes should occur at well-defined frequencies with respect to the fundamental mode. Figure 2c shows a comparison of the predicted and measured frequencies and eigenmodes of the higher order modes, and the predicted resonances are shown as red dotted lines in Figure 2b. A pair of indices, (n, m), describe the eigenmodes in a circular 2D membrane. The first index (n) represents the azimuthal node number, and the second index (m) represents the radial node number. Rather than resonances appearing at exactly the predicted value, two resonances are consistently observed just above and below. For example, the (1,1) degenerate eigenmode, is predicted to be at 24.82 MHz, between the measured resonances at 22.5 and 26.3 MHz. This behavior can be explained by a splitting of degenerate modes within the resonator and is also seen in monolayer and few-layer 2D resonators.[6,47,48] To confirm that the splitting is due to a breaking of symmetry, we measured the eigenmodes of each resonance. As seen in Figure 2c, the eigenmode shapes of the two measured resonances are the same as the predicted (1,1) eigenmode but vibrate along different directions. This indicates that there is anisotropic tension within the membrane, with higher tension along the x direction than the y direction. Given

DOI: 10.1021/acs.nanolett.8b01926
Nano Lett. XXXX, XXX, XXX−XXX

the anisotropic clamping, ripples, and bubbles observed in the AFM images, it is not surprising to see an impact on the eigenmode shape.[49] Similar splitting and distortion are visible in the predicted versus measured (2,1) and (0,2) eigenmodes; however, for higher modes, it becomes more difficult to quantify the impact of anisotropic strain on mode shape and frequency. These results show that 2D bimorphs still behave as anisotropically tensioned membranes, similar to monolayer and few-layer resonators despite the breaking of the out-of-plane symmetry within the heterostructure.

Figure 3 focuses on the noise floor, dynamic range, and nonlinear response of the 2D bimorph to drive. The spectrum analyzer was utilized for measuring the driven and thermal vibrations. When measuring thermal vibrations, the output signal from the spectrum analyzer was turned off. The bandwidth and step size of the two measurements were kept the same (1 kHz). Figure 3a is the noise power density measured at a bandwidth of 1 kHz in units of square picometers per hertz. The black line is a fit to the noise power density function $S_{ZZ}(f)$ described below. Figure 3b shows the resonator response versus RF drive at fixed laser power of 50 μW and a fixed gate voltage of V_{DC} = 15 V. Figure 3c shows the amplitude of motion at resonance versus drive, while the inset shows the small drive response. In Figure 3c, the resonator amplitude displays a linear dependence for drive less than 100 mV before an onset of hardening and Duffing nonlinear dependence at a large drive. As shown in Figure S4, all measured devices show similar behavior.

The minimum drive is limited by the Brownian motion of the resonator at f_0 and the measurement bandwidth (Figure 3a), which is fully determined by statistical mechanics.[50] The thermal noise power density of a mechanical resonator is:

$$S_{ZZ}(f) = \frac{k_B T f_0}{2\pi^3 m_{eff} Q[(f^2 - f_0^2)^2 + (ff_0/Q)^2]} \quad (1)$$

where k_B is the Boltzmann constant, T is the ambient temperature, Q is the quality factor, and f_0 is the resonance frequency. The effective mass, $m_{eff} = 0.2695\pi r^2 \rho$ is determined from the electrostatic tuning discussed later in Figure 4. By comparing the signal level of the Brownian motion to the driven motion at the same bandwidth, we calibrate the measured laser response to picometers (see section 2 of the Supporting Information).[3,50]

The onset of nonlinearity at large drive is determined by the critical amplitude a_C, defined as the onset of bistability.[51,52] Using the calibrated response, we directly extract the critical amplitude from Figure 3b, a_c = 780 pm. The amplitude response determines the dynamic range of the resonator, which is defined as the number of decades between the minimum measurable signal and onset of nonlinearity:[51,52]

$$DR \equiv 20 \log\left(\frac{0.745 a_c}{\sqrt{2S_{x,th}(f_0)BW}}\right) \quad (2)$$

eq 2 yields a dynamic range of 44 dB at a bandwidth of 1 kHz. The obtained dynamic range for the 2D bimorph is comparable to 2D resonators from monolayer or multilayer graphene or MoS_2 in literature, which range from ~40 to 110 dB.[6,52,53]

Figure 3d shows the extracted resonance full width at half-maximum (fwhm) versus drive, which is a measure of dissipation in the resonator. While the fwhm remains constant for large drive, it decreases by nearly a factor of 2 with a linear amplitude dependence at smaller drives (<20 mV), indicating that additional nonlinear processes contribute to the membrane mechanics beyond Duffing mechanics. The laser-power-

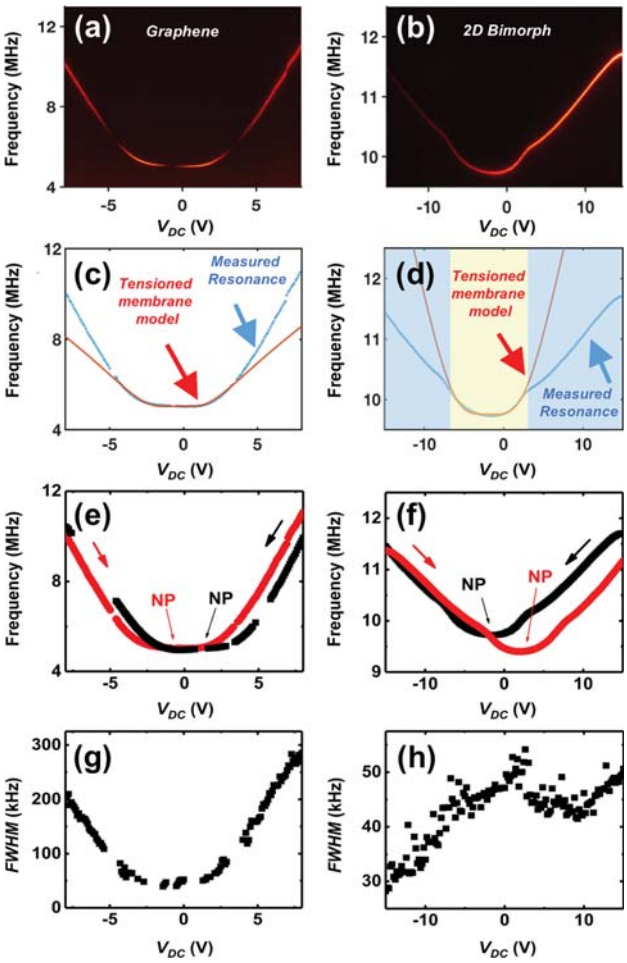

Figure 4. Electrostatic frequency tuning of the fundamental mode in a graphene resonator vs a 2D bimorph resonator. (a, b) Measured amplitude of motion vs frequency and electrostatic gate voltage for a graphene resonator and 2D bimorph, respectively. The electrostatic gate tensions the membranes, giving the frequency tuning of the resonators. The data was measured by sweeping the frequency in a spectrum analyzer to get a resonance mode like the ones in Figures 2 and 3 and then stepping the gate voltage. Color scale is the measured dynamic optical reflectance, which is a convolution of amplitude of motion and changes in the optical interferometric path.[18] (c, d) Resonance frequency vs gate voltage from the tuning data of graphene and 2D bimorph, respectively (blue). The resonance was fit with a Lorentzian at each gate value to extract the frequency and peak width. The tensioned membrane model was applied to fit the tuning curve (orange). The tensioned membrane model is only valid in the low-voltage region. At higher gate voltages, the data starts to deviate from the model. The graphene resonator shows strong hardening behavior, whereas the 2D bimorph shows strong softening behavior with a kink. (e, f) Extracted resonance frequency while sweeping gate voltage up (red curve) vs down (black curve) for graphene and the 2D bimorph. A shift in frequency between the up- and down-sweeps indicates hysteresis in the measured mechanical resonance, indicating that the membrane tensioning is inelastic. (g, h) Extracted fwhm, which is a measure of dissipation within the resonator, vs electrostatic gate V_{DC} for the graphene and 2D bimorph, respectively. In the graphene resonator, the fwhm is symmetric around the neutral point (NP), while in the 2D bimorph, there is an asymmetry in tuning between the negative and positive gate voltages.

DOI: 10.1021/acs.nanolett.8b01926
Nano Lett. XXXX, XXX, XXX−XXX

dependent fwhm of the 2D bimorph shows the same trend (see Figure S5). The origin of these nonlinearities is under intense study in monolayer and few-layer membranes and is still poorly understood.[17]

Figure 4 focuses on the electrostatic tunability of both a monolayer graphene and 2D bimorph drumhead resonators. The graphene resonator is used as a reference to establish the new behavior observed in the bimorph. Figure 4a,b show the dynamic reflected laser response, proportional to the amplitude of motion of the resonators versus DC electrostatic gate voltage and drive frequency. The electrostatic voltage pulls down on the graphene and 2D bimorph membranes, causing it to stretch and tense. A key feature of 2D material resonators is their exceptional tunability due to their unbeatable thickness. For example, the graphene resonator in Figure 4a shows a room temperature tunability of >100% over a gate range of ±8 V and a symmetric measured signal amplitude. Similar tunability is found for other graphene resonators in the literature, although the exact values change dramatically with geometry, capacitance, and temperature.[4,5,7,16] In contrast, we observe four surprising features in the frequency tunability of the 2D bimorph. First, there are distinct kinks in the tuning occurring at gate voltages $V_{DC} = -7.4$ V and +2.8 V. Second, the tunability of the bimorph is only ~20% over a gate range of ±15 V. Third, there is strong hysteresis in the tuning depending on the direction of sweep of the gate voltage. Fourth, there is an asymmetry in the measured signal amplitude for negative versus positive gate voltages. A total of three other 2D bimorph devices show similar kinks and tunability (see Figure S6). Because frequency tuning is inherently a nonlinear process, there are many nonlinear features that emerge in monolayer and few layer 2D resonators, like tensioning, capacitive softening and mode coupling like avoided crossings.[4,7,54,55] As discussed further below, the kinks observed here are distinct from any of these previously observed nonlinearities and represent new features in the 2D bimorph not seen in monolayer and few-layer resonators.

Figure 4c,d compares the extracted resonance frequencies versus gate voltage to the value predicted by a tensioned membrane model with a capacitive softening correction. This model is commonly used to describe the tuning behavior of monolayer and few-layer 2D atomic membranes.[18] Graphene and MoS_2 have, respectively, a 2D Young's modulus and density of 340 N/m and 7.4×10^{-7} kg/m^2 versus 180 N/m and 3.3×10^{-6} kg/m^2.[1,2] For the purposes of comparison, we apply the simplest assumption that the membrane is under equal biaxial strain, and then the Young's modulus and density will add linearly to give $E_{bimorph} = 520$ N/m and 4.04×10^{-6} kg/m^2 Under this model, the tuning of a circular atomic membrane should follow the relation in eq 3:[18]

$$\left(f^2 - A_3(V_g - \Delta\varnothing)^2 - \frac{2.404^2 E\varepsilon_0}{4\pi^2 r^2 \rho}\right)(f^2 - A_3(V_g - \Delta\varnothing)^2)^2 = \frac{2.404^6 \varepsilon_0^2 E}{6144\pi^6 r^4 d^4 \rho^3 1 - \nu}(V_g - \Delta\varnothing)^4 \quad (3)$$

where E is elastic modulus of the membrane, ε_0 is initial strain, r is the radius of the hole, ρ is the density of the membrane ($\alpha \times \rho_{graphene+MoS_2}$), $\Delta\varnothing$ is the work function difference between 2D bimorph and silicon gate, V_g is DC gate voltage, ν is the Poisson's ratio, f is the resonance frequency, and A_3 is the correction term for capacitive softening. Fitting eq 3 to the tuning data yields the initial strain in the membrane ε_0 and the additional absorbed mass factor α, due to fabrication residue or gas trapped at the interface. This model predicts that the behavior of the resonator is symmetric around the minimum work function $\Delta\varnothing$, elastic, and continuously varying. There have been reports in the literature that ripples and wrinkles significantly lower the effective elastic modulus in suspended atomic membranes.[56] Accounting for this softening will affect the numerical values but not the shape of the curve. There is no complete model that unravels the contributions from this softening versus the new mechanisms arising in a heterostructure, so, for the purposes of this study, we applied the simplest assumption of a uniform tension.

To get the curve in Figure 4c,d, the tensioned membrane model is fit to the frequency tuning at low gate voltage of <±5 V. For the graphene resonator (Figure 4c), the model generates the obtained density factor of $\alpha = 17.6$ and initial 2D strain of $\varepsilon_0 = 6.0 \times 10^{-5}$. For 2D bimorphs (Figure 4d), the model gives a density factor of $\alpha = 6.35$ and an initial 2D strain of $\varepsilon_0 = 2.9 \times 10^{-4}$. These values are similar to what is measured in monolayer membranes.[16,18] In Figure 4d, this model fits well for small gate voltages, but there are sharp kinks at $V_{DC} = -7.4$ V and +2.8 V, where the measured frequency tuning drops off dramatically compared with the model. While small deviations from the tensioned membrane model are seen in graphene resonators, these typically lead to increased, rather than decreased, frequency tuning, in contrast to what is observed here.[18] Also, these deviations are continuous, without distinct kinks. The graphene resonance data also supports this trend as shown in Figure 4c. Via relation of the kink frequency to the tensioned membrane model, the onset of the deviation at the kinks occurs when the tension in the membrane increased by $\Delta\sigma = 0.014$ N/m, corresponding with a strain of $\Delta\varepsilon = 2.7 \times 10^{-5}$, a factor of 10 lower than the initial stress and strain of the membrane. Table S1 summarizes the fit parameters for all 2D bimorphs measured and show that all the kinks observed occur at relative stresses $\Delta\sigma$ between 10 and 30 mN/m.

Clearly, the tensioned membrane model fails in the large gate regime, and there appears to be a transition to a new regime. As additional evidence of the failure of the tensioned membrane model, Figure 4e,f shows the frequency tuning in both the graphene and 2D bimorph resonators for both the up-and the down-sweep of gate voltage V_{DC}. In both devices, the frequency tuning displays hysteresis in which the down-sweep from positive to negative gate voltage is different from the up-sweep from negative gate voltage to positive gate voltage. This hysteresis is repeatable, such that repeating the sweep conditions gives the same results. While it is not unusual for electronic devices from nanomaterials to display hysteresis due to a changing electrostatic potential, usually, the electronic hysteresis moves the charge neutrality point in the direction of sweep.[57] This is the behavior seen in the graphene resonator. However, in the 2D bimorph (Figure 4f), exactly the opposite behavior is observed, leading us to conclude that the hysteresis has a different origin. All other measured 2D bimorph devices consistently show the same hysteresis behavior (Figure S7).

Finally, Figure 4g,h shows the resonance fwhm as a function of gate voltage for both the graphene and the 2D bimorph, respectively. The graphene resonator (Figure 4g) shows a symmetric fwhm around the neutrality point, as has been observed previously.[5,58] In contrast, for the 2D bimorph (Figure 4h), there is a broken symmetry with the fwhm a constant for positive gate voltage and decreasing with negative gate voltage. This asymmetry is also reflected in the measured signal

DOI: 10.1021/acs.nanolett.8b01926
Nano Lett. XXXX, XXX, XXX−XXX

amplitude in Figure 4b. However, we note that there is variation in both the asymmetry in amplitude and fwhm from device to device, as shown in Figures S6 and S8. Devices may display higher amplitude at either positive or negative gate voltages. However, the fwhm is consistently broader for larger measured amplitudes.

The exact origin of dissipation in NEMS is notoriously difficult to nail down. We are able to rule out pure optomechanical coupling and piezoelectric dissipation as the origin of the observed asymmetry. First, the graphene resonator shows symmetric behavior, so changes in light intensity due to interferometry from a change in position of the membrane should not be the dominant mechanism in the broken symmetry of amplitude and fwhm. Second, as shown in Figure S8, while there is a shift of both the frequency tuning and fwhm with increasing laser power, and both the kinks and the asymmetry are preserved. As we calculate in Supporting Discussion 4, a simple estimate of joule heating dissipation shows that the piezoelectrically induced currents from MoS_2 will not play a significant role in the dissipation. Instead, we hypothesize that the asymmetry originates from a gate tunable nonlinearity rising from the electronic properties of the MoS_2. MoS_2 is an excitonic n-type semiconductor whose light absorption and conductivity are tuned by varying the electrostatic potential. The gate tunes the conductivity and optical absorption in the MoS_2, leading to a change in the up−down asymmetry and nonlinearity of the bimorph resonator. Under this hypothesis, device to device variations can be explained as variations in the Fermi level of the MoS_2.

There are several mechanisms not included in the tensioned membrane model that could impact the frequency tuning measurements. These contributions are classified by mechanisms that would also impact the tuning of monolayer and few-layer resonators, nonlinear phenomena, or mechanisms unique to heterostructures. In the first class, many phenomena affect the resonance frequency of monolayer atomic membranes, such as gas trapped inside the chamber,[59] ripples and morphology changes,[49,60] and edge adhesion.[61] However, the kinks and hysteresis have not been observed in monolayer and few layer samples, such as the comparison graphene sample shown in Figure 4, suggesting that these conventional mechanisms do not contribute to the new phenomena observed here.

In the second class, frequency tuning is a nonlinear process, leading to nonlinear contributions such as tensioning, capacitive softening, avoided crossings, and thermal stresses from laser heating. Both tensioning and capacitive softening lead to sublinear or even negative tuning of the resonance,[4,18,54,62] but both of these processes are included in the tensioned membrane model and are continuous; they do not explain the sharp kink. Because of the large tunability of 2D resonators, it is common to see nonlinear avoided crossings due to coupling between resonance modes or with external modes from gold clamps or other suspended sections.[4,7,54,55] Avoided crossings occur when two modes cross one another. One of these modes might be invisible due to the position of the laser compared with the eigenmode. However, avoided crossings have a distinctive shape with enhancement of motion and a gap in tuning at the crossover in the resonance frequencies. While the observed kink does bear a resemblance to the kinks observed in avoided crossings, there is no gap and no enhancement, so an avoided crossing is unlikely. Moreover, because of the small tunability of the bimorph compared with monolayer resonators, there is no crossover with other modes. As seen in Figure 2, the higher harmonics are all far outside the tuning range of the first mode, and because of the circular clamping, there should be no external clamping resonances to couple to. Finally, the detection laser may lead to optomechanical back-action and thermal stresses from laser heating. However, as discussed earlier, Figure S8 shows that the kink features are preserved under increasing laser power, suggesting that neither of these mechanisms dominates the tuning behavior.

Finally, the additional mechanisms that will be unique to heterostructures include the following: First, interlayer shear, when combined with the lack of bonds at a van der Waals interface, could result in interlayer slip. Second, the bubbles and folds like those observed in the AFM in Figure 1d may unzip to generate extra length when the membrane is tensioned. Both cases will lead to a softening of the membrane tension, and both adhesion[61] and slip[31] are inelastic phenomena that could lead to hysteresis. However, separating the relative contribution from these two cases is challenging. Incorporating a contribution from slip into the tensioned membrane model is nontrivial. We attempted several adaptations, allowing for free or partial slipping between the layers, but found that none of these models fit the data adequately. We also note that the change in strain of a 6 μm membrane at the onset of slip only corresponds with a 0.2 nm change in the in-plane length. Thus, changes in strain through electrostatic tuning and actuation should not significantly alter the bubble and fold morphology.

We turn to computational simulations to gain insight into the measured strains. As shown in Figure 5, we apply density functional theory to calculate the energy barriers for the onset of slip under interlayer shear of an aligned AB stacked bilayer graphene and a misaligned graphene−MoS_2 heterostructure. These structures represent the extreme cases bounding the slip energy in a 2D heterostructure. The simulations predict that the barrier to slip of an incommensurate heterostructure to be 0.102 mN/m and for a commensurate bilayer to be 35 mN/m. Indeed, the measured tension at the onset of the kink of $\Delta\sigma = 14$ mN/m lies between these two extremes but closer to the energy barrier for an aligned structure. This suggests that either dirt at the interface between the layers or the interlayer folds act to pin or localize slipping, concentrating the forces.

In conclusion, the above devices represent a new class of NEMS from van der Waals heterostructures and represent the ultimate limit of a 2D bimorph. Because the mechanical resonance is highly sensitive to the membrane properties, these devices provide a sensitive probe of the mechanics of a 2D heterostructure and van der Waals interfaces. Due to the atomic-scale thickness, the bending modulus of the 2D bimorph does not dominate the behavior, so in many respects (e.g., well-defined eigenmodes harmonics and large dynamic range), these structures behave as tensioned atomic membranes with no regard to the bimorph structure. However, this simple model breaks down in the frequency tuning of the heterostructure, which deviates strongly from the tensioned membrane model. The exact origin of this deviation is difficult to establish but is likely due to either interlayer slippage or the unzipping of folds between the layers. Further work will need to separate out the relative contributions of membrane morphology, thermal effects on membrane stress and interlayer friction, interface cleanliness, and interlayer bubbles and ripples on the mechanics of these structures. In particular, we need to build a more-complete model, which incorporates these extra interactions to predict membrane behavior.

DOI: 10.1021/acs.nanolett.8b01926
Nano Lett. XXXX, XXX, XXX−XXX

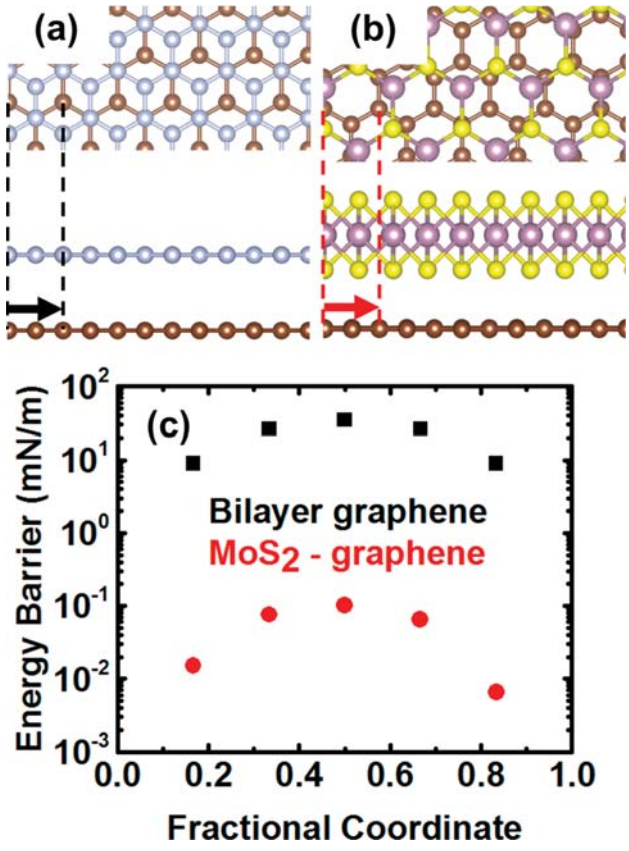

Figure 5. Atomic-scale simulation for slip energy barrier calculation between (a) AB-stacked bilayer graphene and (b) an incommensurate MoS_2−graphene heterostructure. Black and red arrows show the corresponding slip direction and distance. (c) Plot of calculated energy vs interlayer alignment for both systems, giving the energy barrier for slip. Because of the large difference in relative energies, the plot is on a logarithmic scale.

If interlayer slip is occurring, it has major implications on electromechanical devices from 2D heterostructures. If 2D heterostructures can relieve stress through interlayer slip, then 2D heterostructures will behave as ultrapliable films with bending modulus orders of magnitude smaller than in 3D films and devices. Meanwhile, because nearly any electronic device can be made by careful layering of different 2D materials with selected electronic properties, it should be possible to engineer heterostructure devices such as crumpled, strain-resilient electronics[63] or atomic membranes, which couple the electronic or optical properties of 2D heterostructures to the mechanical properties for NEMS with new functionality.

■ ASSOCIATED CONTENT

Supporting Information

The Supporting Information is available free of charge on the ACS Publications website at DOI: 10.1021/acs.nanolett.8b01926.

Additional details on sample fabrication and measurement, calibration of the amplitude of motion, parametric dependence, estimate of piezoelectrically driven Joule heating, and density functional theory parameters (PDF)

■ AUTHOR INFORMATION

Corresponding Authors

*E-mail: skim501@illinois.edu.
*E-mail: arendv@illinois.edu.

ORCID

Arend M. van der Zande: 0000-0001-5104-9646

Author Contributions

A.v.d.Z. and S.P.K. conceived the idea and designed the experiments. S.P.K. conducted material growth, fabrications, and measurements. A.v.d.Z and S.P.K. analyzed the data. J.Y. performed the DFT simulations.

Notes

The authors declare no competing financial interest.

■ ACKNOWLEDGMENTS

This research was partially supported by the National Science Foundation MRSEC program under NSF Award Number DMR-1720633. This work was carried out in the Material Research Laboratory Central Facilities and the Micro and Nano Technology Laboratory. We thank Jangyup Son, Mohammad Abir Hossain, Yunjo Jung, Nikita Buzov, Elif Ertekin, Narayan Aluru, and Pinshane Huang for helpful discussions.

■ REFERENCES

(1) Lee, C.; Wei, X. D.; Kysar, J. W.; Hone, J. Measurement of the elastic properties and intrinsic strength of monolayer graphene. *Science* **2008**, *321* (5887), 385−388.

(2) Bertolazzi, S.; Brivio, J.; Kis, A. Stretching and Breaking of Ultrathin MoS2. *ACS Nano* **2011**, *5* (12), 9703−9709.

(3) Bunch, J. S.; van der Zande, A. M.; Verbridge, S. S.; Frank, I. W.; Tanenbaum, D. M.; Parpia, J. M.; Craighead, H. G.; McEuen, P. L. Electromechanical resonators from graphene sheets. *Science* **2007**, *315* (5811), 490−493.

(4) van der Zande, A. M.; Barton, R. A.; Alden, J. S.; Ruiz-Vargas, C. S.; Whitney, W. S.; Pham, P. H.; Park, J.; Parpia, J. M.; Craighead, H. G.; McEuen, P. L. Large-scale arrays of single-layer graphene resonators. *Nano Lett.* **2010**, *10* (12), 4869−4873.

(5) Morell, N.; Reserbat-Plantey, A.; Tsioutsios, I.; Schadler, K. G.; Dubin, F.; Koppens, F. H.; Bachtold, A. High Quality Factor Mechanical Resonators Based on WSe2Monolayers. *Nano Lett.* **2016**, *16* (8), 5102−5108.

(6) Barton, R. A.; Ilic, B.; van der Zande, A. M.; Whitney, W. S.; McEuen, P. L.; Parpia, J. M.; Craighead, H. G. High, Size-Dependent Quality Factor in an Array of Graphene Mechanical Resonators. *Nano Lett.* **2011**, *11* (3), 1232−1236.

(7) Chen, C.; Rosenblatt, S.; Bolotin, K. I.; Kalb, W.; Kim, P.; Kymissis, I.; Stormer, H. L.; Heinz, T. F.; Hone, J. Performance of monolayer graphene nanomechanical resonators with electrical readout. *Nat. Nanotechnol.* **2009**, *4* (12), 861−867.

(8) Lee, C. H.; Lee, G. H.; van der Zande, A. M.; Chen, W.; Li, Y.; Han, M.; Cui, X.; Arefe, G.; Nuckolls, C.; Heinz, T. F.; Guo, J.; Hone, J.; Kim, P. Atomically thin p−n junctions with van der Waals heterointerfaces. *Nat. Nanotechnol.* **2014**, *9* (9), 676−681.

(9) Dean, C. R.; Young, A. F.; Meric, I.; Lee, C.; Wang, L.; Sorgenfrei, S.; Watanabe, K.; Taniguchi, T.; Kim, P.; Shepard, K. L.; Hone, J. Boron nitride substrates for high-quality graphene electronics. *Nat. Nanotechnol.* **2010**, *5* (10), 722−726.

(10) Wang, L.; Meric, I.; Huang, P. Y.; Gao, Q.; Gao, Y.; Tran, H.; Taniguchi, T.; Watanabe, K.; Campos, L. M.; Muller, D. A.; Guo, J.; Kim, P.; Hone, J.; Shepard, K. L.; Dean, C. R. One-Dimensional Electrical Contact to a Two-Dimensional Material. *Science* **2013**, *342* (6158), 614−617.

(11) Chen, C.; Lee, S.; Deshpande, V. V.; Lee, G. H.; Lekas, M.; Shepard, K.; Hone, J. Graphene mechanical oscillators with tunable frequency. *Nat. Nanotechnol.* **2013**, *8* (12), 923−927.

DOI: 10.1021/acs.nanolett.8b01926
Nano Lett. XXXX, XXX, XXX−XXX

(12) Liu, X.; Suk, J. W.; Boddeti, N. G.; Cantley, L.; Wang, L.; Gray, J. M.; Hall, H. J.; Bright, V. M.; Rogers, C. T.; Dunn, M. L.; Ruoff, R. S.; Bunch, J. S. Large arrays and properties of 3-terminal graphene nanoelectromechanical switches. *Adv. Mater.* **2014**, *26* (10), 1571−1576.
(13) Wu, W.; Wang, L.; Li, Y.; Zhang, F.; Lin, L.; Niu, S.; Chenet, D.; Zhang, X.; Hao, Y.; Heinz, T. F.; Hone, J.; Wang, Z. L. Piezoelectricity of single-atomic-layer MoS2 for energy conversion and piezotronics. *Nature* **2014**, *514* (7523), 470−474.
(14) Weber, P.; Guttinger, J.; Noury, A.; Vergara-Cruz, J.; Bachtold, A. Force sensitivity of multilayer graphene optomechanical devices. *Nat. Commun.* **2016**, *7*, 12496.
(15) Song, X. F.; Oksanen, M.; Sillanpaa, M. A.; Craighead, H. G.; Parpia, J. M.; Hakonen, P. J. Stamp Transferred Suspended Graphene Mechanical Resonators for Radio Frequency Electrical Readout. *Nano Lett.* **2012**, *12* (1), 198−202.
(16) Miao, T. F.; Yeom, S.; Wang, P.; Standley, B.; Bockrath, M. Graphene Nanoelectromechanical Systems as Stochastic-Frequency Oscillators. *Nano Lett.* **2014**, *14* (6), 2982−2987.
(17) Eichler, A.; Moser, J.; Chaste, J.; Zdrojek, M.; Wilson-Rae, I.; Bachtold, A. Nonlinear damping in mechanical resonators made from carbon nanotubes and graphene. *Nat. Nanotechnol.* **2011**, *6* (6), 339−342.
(18) Barton, R. A.; Storch, I. R.; Adiga, V. P.; Sakakibara, R.; Cipriany, B. R.; Ilic, B.; Wang, S. P.; Ong, P.; McEuen, P. L.; Parpia, J. M.; Craighead, H. G. Photothermal Self-Oscillation and Laser Cooling of Graphene Optomechanical Systems. *Nano Lett.* **2012**, *12* (9), 4681−4686.
(19) Miskin, M. Z.; Dorsey, K. J.; Bircan, B.; Han, Y.; Muller, D. A.; McEuen, P. L.; Cohen, I. Graphene-based bimorphs for micron-sized, autonomous origami machines. *Proc. Natl. Acad. Sci. U. S. A.* **2018**, *115* (3), 466−470.
(20) Will, M.; Hamer, M.; Muller, M.; Noury, A.; Weber, P.; Bachtold, A.; Gorbachev, R. V.; Stampfer, C.; Guttinger, J. High Quality Factor Graphene-Based Two-Dimensional Heterostructure Mechanical Resonator. *Nano Lett.* **2017**, *17* (10), 5950−5955.
(21) Dienwiebel, M.; Verhoeven, G. S.; Pradeep, N.; Frenken, J. W. M.; Heimberg, J. A.; Zandbergen, H. W. Superlubricity of graphite. *Phys. Rev. Lett.* **2004**, *92* (12), 1 DOI: 10.1103/PhysRevLett.92.126101.
(22) Leven, I.; Krepel, D.; Shemesh, O.; Hod, O. Robust Superlubricity in Graphene/h-BN Heterojunctions. *J. Phys. Chem. Lett.* **2013**, *4* (1), 115−120.
(23) Hirano, M.; Shinjo, K.; Kaneko, R.; Murata, Y. Anisotropy of Frictional Forces in Muscovite Mica. *Phys. Rev. Lett.* **1991**, *67* (19), 2642−2645.
(24) Alden, J. S.; Tsen, A. W.; Huang, P. Y.; Hovden, R.; Brown, L.; Park, J.; Muller, D. A.; McEuen, P. L. Strain solitons and topological defects in bilayer graphene. *Proc. Natl. Acad. Sci. U. S. A.* **2013**, *110* (28), 11256−11260.
(25) Feng, X. F.; Kwon, S.; Park, J. Y.; Salmeron, M. Superlubric Sliding of Graphene Nanoflakes on Graphene. *ACS Nano* **2013**, *7* (2), 1718−1724.
(26) Li, H.; Wang, J. H.; Gao, S.; Chen, Q.; Peng, L. M.; Liu, K. H.; Wei, X. L. Superlubricity between MoS2 Monolayers. *Adv. Mater.* **2017**, *29* (27). DOI: 10.1002/adma.201770200
(27) Liu, Z.; Yang, J. R.; Grey, F.; Liu, J. Z.; Liu, Y. L.; Wang, Y. B.; Yang, Y. L.; Cheng, Y.; Zheng, Q. S. Observation of Microscale Superlubricity in Graphite. *Phys. Rev. Lett.* **2012**, *108* (20). DOI: 10.1103/PhysRevLett.108.205503
(28) Koren, E.; Lortscher, E.; Rawlings, C.; Knoll, A. W.; Duerig, U. Surface science. Adhesion and friction in mesoscopic graphite contacts. *Science* **2015**, *348* (6235), 679−683.
(29) Wang, L. F.; Zhou, X.; Ma, T. B.; Liu, D. M.; Gao, L.; Li, X.; Zhang, J.; Hu, Y. Z.; Wang, H.; Dai, Y. D.; Luo, J. B. Superlubricity of a graphene/MoS2 heterostructure: a combined experimental and DFT study. *Nanoscale* **2017**, *9* (30), 10846−10853.
(30) Berman, D.; Erdemir, A.; Sumant, A. V. Approaches for Achieving Superlubricity in Two-Dimensional Materials. *ACS Nano* **2018**, *12* (3), 2122−2137.
(31) Wei, X. D.; Meng, Z. X.; Ruiz, L.; Xia, W. J.; Lee, C.; Kysar, J. W.; Hone, J. C.; Keten, S.; Espinosa, H. D. Recoverable Slippage Mechanism in Multilayer Graphene Leads to Repeatable Energy Dissipation. *ACS Nano* **2016**, *10* (2), 1820−1828.
(32) Benameur, M. M.; Gargiulo, F.; Manzeli, S.; Autes, G.; Tosun, M.; Yazyev, O. V.; Kis, A. Electromechanical oscillations in bilayer graphene. *Nat. Commun.* **2015**, *6*. DOI: 10.1038/ncomms9582
(33) Liu, K.; Yan, Q. M.; Chen, M.; Fan, W.; Sun, Y. H.; Suh, J.; Fu, D. Y.; Lee, S.; Zhou, J.; Tongay, S.; Ji, J.; Neaton, J. B.; Wu, J. Q. Elastic Properties of Chemical-Vapor-Deposited Monolayer MoS2, WS2, and Their Bilayer Heterostructures. *Nano Lett.* **2014**, *14* (9), 5097−5103.
(34) Ye, F.; Lee, J.; Feng, P. X. Atomic layer MoS2-graphene van der Waals heterostructure nanomechanical resonators. *Nanoscale* **2017**, *9* (46), 18208−18215.
(35) van der Zande, A. M.; Huang, P. Y.; Chenet, D. A.; Berkelbach, T. C.; You, Y. M.; Lee, G. H.; Heinz, T. F.; Reichman, D. R.; Muller, D. A.; Hone, J. C. Grains and grain boundaries in highly crystalline monolayer molybdenum disulphide. *Nat. Mater.* **2013**, *12* (6), 554−561.
(36) Ling, X.; Lee, Y. H.; Lin, Y. X.; Fang, W. J.; Yu, L. L.; Dresselhaus, M. S.; Kong, J. Role of the Seeding Promoter in MoS2 Growth by Chemical Vapor Deposition. *Nano Lett.* **2014**, *14* (2), 464−472.
(37) Li, X. S.; Cai, W. W.; An, J. H.; Kim, S.; Nah, J.; Yang, D. X.; Piner, R.; Velamakanni, A.; Jung, I.; Tutuc, E.; Banerjee, S. K.; Colombo, L.; Ruoff, R. S. Large-Area Synthesis of High-Quality and Uniform Graphene Films on Copper Foils. *Science* **2009**, *324* (5932), 1312−1314.
(38) Rosenberger, M. R.; Chuang, H. J.; McCreary, K. M.; Hanbicki, A. T.; Sivaram, S. V.; Jonker, B. T. Nano-"Squeegee" for the Creation of Clean 2D Material Interfaces. *ACS Appl. Mater. Interfaces* **2018**, *10* (12), 10379−10387.
(39) Buscema, M.; Steele, G. A.; van der Zant, H. S. J.; Castellanos-Gomez, A. The effect of the substrate on the Raman and photoluminescence emission of single-layer MoS2. *Nano Res.* **2014**, *7* (4), 561−571.
(40) Tien, D. H.; Park, J. Y.; Kim, K. B.; Lee, N.; Choi, T.; Kim, P.; Taniguchi, T.; Watanabe, K.; Seo, Y. Study of Graphene-based 2D-Heterostructure Device Fabricated by All-Dry Transfer Process. *ACS Appl. Mater. Interfaces* **2016**, *8* (5), 3072−3078.
(41) Khestanova, E.; Guinea, F.; Fumagalli, L.; Geim, A. K.; Grigorieva, I. V. Universal shape and pressure inside bubbles appearing in van der Waals heterostructures. *Nat. Commun.* **2016**, *7*, 12587.
(42) Novoselov, K. S.; Mishchenko, A.; Carvalho, A.; Castro Neto, A. H. 2D materials and van der Waals heterostructures. *Science* **2016**, *353* (6298), aac9439.
(43) Argentero, G.; Mittelberger, A.; Monazam, M. R. A.; Cao, Y.; Pennycook, T. J.; Mangler, C.; Kramberger, C.; Kotakoski, J.; Geim, A. K.; Meyer, J. C. Unraveling the 3D Atomic Structure of a Suspended Graphene/hBN van der Waals Heterostructure. *Nano Lett.* **2017**, *17* (3), 1409−1416.
(44) Haigh, S. J.; Gholinia, A.; Jalil, R.; Romani, S.; Britnell, L.; Elias, D. C.; Novoselov, K. S.; Ponomarenko, L. A.; Geim, A. K.; Gorbachev, R. Cross-sectional imaging of individual layers and buried interfaces of graphene-based heterostructures and superlattices. *Nat. Mater.* **2012**, *11* (9), 764−767.
(45) Kretinin, A. V.; Cao, Y.; Tu, J. S.; Yu, G. L.; Jalil, R.; Novoselov, K. S.; Haigh, S. J.; Gholinia, A.; Mishchenko, A.; Lozada, M.; Georgiou, T.; Woods, C. R.; Withers, F.; Blake, P.; Eda, G.; Wirsig, A.; Hucho, C.; Watanabe, K.; Taniguchi, T.; Geim, A. K.; Gorbachev, R. V. Electronic Properties of Graphene Encapsulated with Different Two-Dimensional Atomic Crystals. *Nano Lett.* **2014**, *14* (6), 3270−3276.
(46) Sanchez, D. A.; Dai, Z. H.; Wang, P.; Cantu-Chavez, A.; Brennan, C. J.; Huang, R.; Lu, N. S. Mechanics of spontaneously formed nanoblisters trapped by transferred 2D crystals. *Proc. Natl. Acad. Sci. U. S. A.* **2018**, *115* (31), 7884−7889.

DOI: 10.1021/acs.nanolett.8b01926
Nano Lett. XXXX, XXX, XXX−XXX

(47) Davidovikj, D.; Slim, J. J.; Cartamil-Bueno, S. J.; van der Zant, H. S. J.; Steeneken, P. G.; Venstra, W. J. Visualizing the Motion of Graphene Nanodrums. *Nano Lett.* **2016**, *16* (4), 2768−2773.
(48) Wang, Z.; Jia, H.; Zheng, X. Q.; Yang, R.; Ye, G. J.; Chen, X. H.; Feng, P. X. Resolving and Tuning Mechanical Anisotropy in Black Phosphorus via Nanomechanical Multimode Resonance Spectromicroscopy. *Nano Lett.* **2016**, *16* (9), 5394−5400.
(49) Garcia-Sanchez, D.; van der Zande, A. M.; Paulo, A. S.; Lassagne, B.; McEuen, P. L.; Bachtold, A. Imaging mechanical vibrations in suspended graphene sheets. *Nano Lett.* **2008**, *8* (5), 1399−1403.
(50) Hauer, B. D.; Doolin, C.; Beach, K. S. D.; Davis, J. P. A general procedure for thermomechanical calibration of nano/micro-mechanical resonators. *Ann. Phys.* **2013**, *339*, 181−207.
(51) Postma, H. W. C.; Kozinsky, I.; Husain, A.; Roukes, M. L. Dynamic range of nanotube- and nanowire-based electromechanical systems. *Appl. Phys. Lett.* **2005**, *86* (22), 223105.
(52) Wang, Z. H.; Feng, P. X. L. Dynamic range of atomically thin vibrating nanomechanical resonators. *Appl. Phys. Lett.* **2014**, *104* (10), 103109.
(53) Feng, P. X. L.; Wang, Z. H.; Lee, J. S.; Yang, R.; Zheng, X.; He, K. L.; Shan, J. Two-Dimensional Nanoelectromechanical Systems (2D NEMS) via Atomically-Thin Semiconducting Crystals Vibrating at Radio Frequencies. *Int. El Devices Meet* **2014**, 811.
(54) Guttinger, J.; Noury, A.; Weber, P.; Eriksson, A. M.; Lagoin, C.; Moser, J.; Eichler, C.; Wallraff, A.; Isacsson, A.; Bachtold, A. Energy-dependent path of dissipation in nanomechanical resonators. *Nat. Nanotechnol.* **2017**, *12* (7), 631−636.
(55) Mathew, J. P.; Patel, R. N.; Borah, A.; Vijay, R.; Deshmukh, M. M. Dynamical strong coupling and parametric amplification of mechanical modes of graphene drums. *Nat. Nanotechnol.* **2016**, *11* (9), 747−751.
(56) Ruiz-Vargas, C. S.; Zhuang, H. L. L.; Huang, P. Y.; van der Zande, A. M.; Garg, S.; McEuen, P. L.; Muller, D. A.; Hennig, R. G.; Park, J. Softened Elastic Response and Unzipping in Chemical Vapor Deposition Graphene Membranes. *Nano Lett.* **2011**, *11* (6), 2259−2263.
(57) Wang, H.; Wu, Y.; Cong, C.; Shang, J.; Yu, T. Hysteresis of electronic transport in graphene transistors. *ACS Nano* **2010**, *4* (12), 7221−7228.
(58) Lee, J.; Wang, Z.; He, K.; Yang, R.; Shan, J.; Feng, P. X. Electrically tunable single- and few-layer MoS2 nanoelectromechanical systems with broad dynamic range. *Sci. Adv.* **2018**, *4* (3), eaao6653.
(59) Bunch, J. S.; Verbridge, S. S.; Alden, J. S.; van der Zande, A. M.; Parpia, J. M.; Craighead, H. G.; McEuen, P. L. Impermeable atomic membranes from graphene sheets. *Nano Lett.* **2008**, *8* (8), 2458−2462.
(60) Bao, W. Z.; Miao, F.; Chen, Z.; Zhang, H.; Jang, W. Y.; Dames, C.; Lau, C. N. Controlled ripple texturing of suspended graphene and ultrathin graphite membranes. *Nat. Nanotechnol.* **2009**, *4* (9), 562−566.
(61) Lloyd, D.; Liu, X. H.; Boddeti, N.; Cantley, L.; Long, R.; Dunn, M. L.; Bunch, J. S. Adhesion, Stiffness, and Instability in Atomically Thin MoS2 Bubbles. *Nano Lett.* **2017**, *17* (9), 5329−5334.
(62) Weber, P.; Guttinger, J.; Tsioutsios, I.; Chang, D. E.; Bachtold, A. Coupling Graphene Mechanical Resonators to Superconducting Microwave Cavities. *Nano Lett.* **2014**, *14* (5), 2854−2860.
(63) Kang, P.; Wang, M. C.; Knapp, P. M.; Nam, S. Crumpled Graphene Photodetector with Enhanced, Strain-Tunable, and Wavelength-Selective Photoresponsivity. *Adv. Mater.* **2016**, *28* (23), 4639−4645.

DOI: 10.1021/acs.nanolett.8b01926
Nano Lett. XXXX, XXX, XXX−XXX